Chen et al. *NPG Asia Materials* (2018) 10: 810–820
DOI 10.1038/s41427-018-0078-6

NPG Asia Materials

ARTICLE Open Access

Degradation behaviors and mechanisms of MoS_2 crystals relevant to bioabsorbable electronics

Xiang Chen[1], Sachin M. Shinde[1], Krishna P. Dhakal[1], Suk Woo Lee[2], Hyunmin Kim[3], Zonghoon Lee[2] and Jong-Hyun Ahn[1]

Abstract

Monolayer molybdenum disulfide (MoS_2) exhibits unique semiconducting and bioresorption properties, giving this material enormous potential for electronic/biomedical applications, such as bioabsorbable electronics. In this regard, understanding the degradation performance of monolayer MoS_2 in biofluids allows modulation of the properties and lifetime of related bioabsorbable devices and systems. Herein, the degradation behaviors and mechanisms of monolayer MoS_2 crystals with different misorientation angles are explored. High-angle grain boundaries (HAGBs) biodegrade faster than low-angle grain boundaries (LAGBs), exhibiting degraded edges with wedge and zigzag shapes, respectively. Triangular pits that formed in the degraded grains have orientations opposite to those of the parent crystals, and these pits grow into larger pits laterally. These behaviors indicate that the degradation is induced and propagated based on intrinsic defects, such as grain boundaries and point defects, because of their high chemical reactivity due to lattice breakage and the formation of dangling bonds. High densities of dislocations and point defects lead to high chemical reactivity and faster degradation. The structural cause of MoS_2 degradation is studied, and a feasible approach to study changes in the properties and lifetime of MoS_2 by controlling the defect type and density is presented. The results can thus be used to promote the widespread use of two-dimensional materials in bioabsorption applications.

INTRODUCTION

Molybdenum disulfide (MoS_2), a key member of the class of materials known as layered transition metal dichalcogenides (TMDCs), has attracted tremendous interest from the scientific community over the past few years because of its applications in various areas, including electronics, optoelectronics, and physicochemical and biomedical sensors[1–7]. In particular, large-scale monolayer MoS_2 synthesized via chemical vapor deposition (CVD) represents an ideal choice for fabricating active semiconducting channels for diodes, transistors, sensors, and other related systems[8–11].

Monolayer MoS_2 can be slowly oxidized in air or dissolved in aqueous solution after several weeks or months, resulting in its environmental degradation[12–15]. Owing to these characteristics, monolayer MoS_2 is an ideal candidate for use in bioabsorbable electronics, such as temporary biomedical sensors and therapeutic vehicles, that can be absorbed after being implanted into the human body, thereby eliminating the need for secondary surgeries to extract the implants[16–19]. The long-term cytotoxicity and immunological biocompatibility of CVD-grown monolayer MoS_2 in biofluids and tissues of live animal models have been reported[20]. Monolayer MoS_2-based bioabsorbable and multifunctional sensors

Correspondence: Jong-Hyun Ahn (ahnj@yonsei.ac.kr)
[1]School of Electrical and Electronic Engineering, Yonsei University, 50 Yonsei-ro, Seodaemun-gu, Seoul 03722, Republic of Korea
[2]School of Materials Science and Engineering, Ulsan National Institute of Science and Technology (UNIST), 50 UNIST-gil, Ulju-gun, Ulsan 44919, Republic of Korea
Full list of author information is available at the end of the article.
These author contributed equally: Xiang Chen, Sachin M. Shinde

for the temporary intracranial monitoring of pressure, temperature, strain, and motion in animal models have also been demonstrated[20]. Such technologies play specific, clinically relevant roles in short-term diagnostic/therapeutic functions during recovery from traumatic brain injuries, but the details and structural cause of monolayer MoS_2 degradation are not so clear.

A fundamental understanding of the degradation behaviors and mechanisms of monolayer MoS_2 in biofluids is therefore critical to maximizing the potential benefit of such materials in a bioabsorbable electronic platform. Thermal oxidation and anisotropic etching of two-dimensional (2D) MoS_2 in air have been previously reported; however, the degradation environment differs substantially from that in biofluids not only with respect to the reaction temperature and speed but also with respect to the reactants and products[12–15,21–25]. Other studies have reported the dissolution of chemically/mechanically exfoliated MoS_2 nanosheets in aqueous solution; however, nanosheets dispersed in solution have little relevance to electronics[26,27]. Fundamental studies, including the interaction between monolayer MoS_2 crystals and biofluids, the morphological evolution, and the role of grain boundaries (GBs) and point defects during degradation, have yet to be adequately conducted [6,26–29].

This study investigates the degradation behaviors and mechanisms of monolayer MoS_2 crystals with different crystallographic misorientation angles in phosphate-buffered saline (PBS) solution. Monolayer crystals are chosen because their basic structure enables rapid degradation and trend analysis. The results show that high-angle grain boundaries (HAGBs, >15°) preferentially degraded faster than low-angle grain boundaries (LAGBs, <15°); this phenomenon, which has not been previously reported, is referred to as "angle-dependent selective degradation." Such selective degradation results from the different dislocation types and defect densities of LAGBs and HAGBs. The degraded LAGBs and HAGBs exhibit wedge- and zigzag-shaped edges, respectively. MoS_2 grains degrade and gradually disappear from the substrate. Triangular pits generated in the degraded MoS_2 grains are oriented opposite to those of parent crystals and grow into larger pits, indicating that the degradation of monolayer MoS_2 is induced by the intrinsic defects and can be extended laterally. High densities of dislocations and point defects (e.g., 5|7-fold or 4|4-fold ring cores, monosulfur vacancies (V_S), or disulfur vacancies (V_{S2})) lead to high chemical reactivity and fast degradation. Herein, a comprehensive study of the degradation of monolayer MoS_2 is presented; the properties and lifetime of 2D MoS_2 in biofluids are controlled by modulation of the defect type and density; and 2D TMDCs are promoted as outstanding candidates for biomedical applications, such as implantable, biocompatible, and bioabsorbable devices and systems in the body.

Materials and methods

Synthesis of monolayer MoS_2 crystals

The atmospheric pressure CVD method was used to synthesize monolayer MoS_2 crystals. First, an SiO_2 (300 nm)/Si substrate was cleaned in acetone, isopropyl alcohol, and deionized (DI) water for 10 min each. Second, the SiO_2/Si substrate was further treated in Piranha solution at 70 °C for 2 h to hydrophilize the surface, and a 5 μM aqueous solution of perylene-3,4,9,10-tetracarboxylic acid tetrapotassium salt (PTAS) was spin-coated as a seeding promoter. Third, 10 mg of MoO_3 powder (99.5%, Sigma-Aldrich) was placed in a ceramic boat and inserted into a single-zone furnace together with the upside-down SiO_2/Si substrate on the boat. In addition, sulfur powder (99.5%, Sigma-Aldrich) was placed on another boat and loaded upstream in the furnace. The furnace was heated to 750 °C within 15 min, maintained at 750 °C for 30 min, and then allowed to naturally cool to room temperature. The synthesis process was protected from air and performed in an atmosphere composed of a mixture of Ar (50 sccm) and H_2 (7.5 sccm) gas.

Degradation of monolayer MoS_2 crystals

Degradation tests of monolayer MoS_2 crystals were performed in PBS solution. Notably, both Si and SiO_2 can dissolve in PBS solution after a period, resulting in MoS_2 crystals detaching from the substrate. To thoroughly study the morphological change of the MoS_2 crystals during the degradation process, the MoS_2 crystals were transferred from SiO_2/Si to an SU-8/sapphire substrate because SU-8/sapphire is more stable in PBS solution.

First, a cleaned sapphire substrate was spin-coated with SU-8 (10% at 3500 rpm; MicroChem), followed by soft baking for 5 min at 65 °C, 2 min of UV treatment, and 30 min of hard baking at 150 °C to attain a thin, smooth SU-8 layer (thickness: ~100 nm; root-mean-square (RMS) roughness: ~0.258 nm). Second, the MoS_2 crystals were spin-coated with poly(methyl methacrylate) (PMMA) and transferred onto the SU-8/sapphire substrate using the wet transfer method. After the film had completely dried, the PMMA layer was carefully removed with hot and room temperature acetone continuously. As a result, MoS_2 crystals were transferred to the target substrate. To study the degradation process and behavior of monolayer MoS_2 crystals in PBS solution, the degradation test was performed in 60 mL of 1.0 M PBS (Sigma-Aldrich) on a hot plate, and the PBS solution was changed every 2 days to maintain its concentration. Finally, an accelerated degradation test was performed in PBS solution (pH 7.4) at 75 °C for 1–7 weeks; the degraded MoS_2 samples were then removed from the PBS solution, rinsed with DI water, and gently blown dry using N_2 gas. As a reference, normal degradation was also investigated in PBS solution (pH 7.4) at 40 °C over 14–28 weeks.

Characterization of monolayer MoS_2 crystals

To investigate the morphological evolution of MoS_2 crystals before and after degradation in PBS solution, optical microscopy (OM) images were captured using a Nikon Eclipse LV100ND microscope. Atomic force microscopy (AFM) images were recorded on a Park system NX10 in noncontact mode. Moreover, Raman and photoluminescence (PL) measurements were performed with a UniNanoTech Uni-RAM2 at a laser excitation wavelength of 532 nm and a laser power of 0.4 mW. To reveal the distribution of GBs between adjacent MoS_2 crystals, second-harmonic generation (SHG) nonlinear optical images were captured using a dual-mode Er-doped fiber laser (Insight Deepsee Dual; Spectra-Physics) and a confocal microscope (IX83; Olympus) after the two spatially overlapped beams were directed to a galvanometric x–y directional mirror controlled by a scanning system (Fluoview1000; Olympus). Furthermore, dark-field transmission electron microscopy (DF-TEM) images were acquired using an image aberration-corrected Titan Cube G2 operated at 80 kV. To avoid damage accumulation, the acquisition time was reduced as magnification increased. HAADF-scanning transmission electron microscopy (STEM) images were obtained with a probe aberration corrector at 80 kV. The accelerated voltage was below the knock-on threshold energy to damage MoS_2.

Results and discussion

The degradation test in this study included four steps, as shown in Fig. 1a. First, monolayer MoS_2 crystals were synthesized on an SiO_2/Si substrate via the CVD method. Second, the crystals were transferred to an SU-8/sapphire substrate. Third, the MoS_2 samples were placed in PBS solution for approximately 7 weeks. Finally, the MoS_2 samples were removed from the PBS solution, carefully cleaned, and characterized. Further details are provided in the Materials and methods section. Note that the SU-8 layer exhibited a smooth surface and high stability in the PBS solution, which contributes to the morphological study of MoS_2 crystals before and after degradation. In addition, the wet transfer process negligibly affected the quality of the MoS_2 crystals. Figure 1b shows the OM images of MoS_2 crystals on SiO_2/Si and SU-8/sapphire substrates. Except for the change in contrast, the crystal surface was smooth and did not show any wrinkles or microcracks. The RMS roughness of the MoS_2 crystals increased (during the transfer process) from 0.20 to 0.62 nm because of the residual PMMA (Supplementary Figure S1). Raman and PL spectra further indicated that the monolayer nature of MoS_2 crystals was maintained after the transfer process because the difference in frequency between the E_{2g} and A_{1g} modes was maintained at 20 cm^{-1} (Fig. 1c). In addition, the crystals were free from doping or strain effects, as indicated by the unchanged PL peak at 1.81 eV (Fig. 1d)[8]. In other words, high-quality CVD-grown monolayer MoS_2 crystals with clean and smooth surfaces were successfully transferred to the SU-8/sapphire substrate.

For CVD-grown monolayer MoS_2 crystals, GBs are inevitably generated between two adjacent grains with crystallographic misorientation[30–34]. In general, LAGBs have a misorientation angle <~15°, whereas HAGBs have an angle >~15°[35]. Because of the hexagonal atomic structure of semiconducting MoS_2 in the 2H phase, the misorientation angle ranges from 0° to 60°[33,36]. The atomic defect structures in MoS_2 grains and GBs greatly affect the mechanical, electrical, and optoelectronic properties of MoS_2-based devices[35,37–43]. To thoroughly explore the degradation behaviors of MoS_2 grains and GBs with different inter-grain misorientation angles, we selected four samples with different angles and characterized their original morphologies and structures. Figure 1e, f show the OM and AFM images of the four samples. These crystals are well attached to the SU-8 layer with a clean surface; however, the GBs cannot be observed in these OM and AFM images due to technical limitations. To visualize the GBs, destructive methods are commonly used, including oxidation in air, ultraviolet light irradiation along with moisture exposure, spin-coating of liquid crystals, and stacking of bilayers[9,36,44,45]. Here, SHG microscopy is used as a nondestructive method to determine the crystalline orientations and the distribution of GBs[46]. Because SHG is highly sensitive to the structural symmetry, MoS_2 crystals with different orientations show different SHG responses, enabling visual distinction of GBs with two anisotropic grains (Fig. 1g)[33]. Notably, the shape of GBs depends on the relative growth rates of the two adjacent edges, which are not easily distinguished in SHG images when the misorientation angle approaches 0° or 60° because of the 60° periodicity caused by the six-fold rotational symmetry of the MoS_2 lattice[33–35]. As demonstrated later, such a simple method of confirming the GBs enables the analysis of degradation processes.

According to previous studies, the dissolution rate of monolayer MoS_2 or Si nanomembranes increases with increasing PBS temperature[20,47]. In view of the dissolution kinetics of monolayer MoS_2 (~200 nm grain size) in PBS solution, a high concentration, pH, or temperature results in a high dissolution speed[20]. Therefore, an accelerated degradation test of CVD-grown monolayer MoS_2 crystals with different misorientation angles is performed in PBS solution (pH 7.4) at 75 °C instead of 37 °C, thereby eliminating the need for longer degradation time in the laboratory[20]. The corresponding OM and AFM images of MoS_2 crystals placed in the PBS solution for 1–7 weeks are shown in Fig. 2a, b. After 1 week, the MoS_2 GBs with misorientation angles of 26°, 40°, or 45° were degraded,

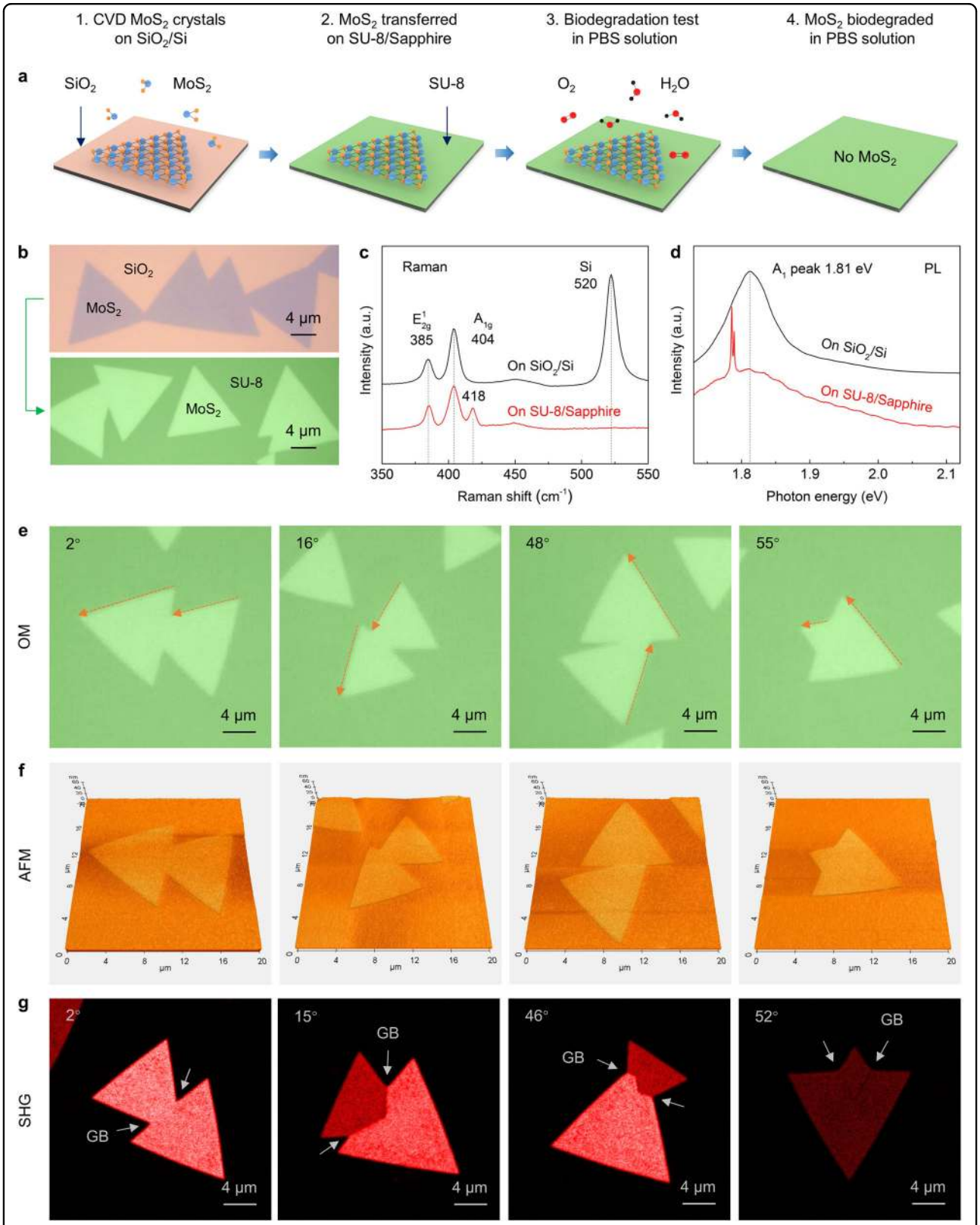

Fig. 1 CVD-grown monolayer MoS_2 crystals with different crystallographic misorientation angles before degradation. a Schematics of the synthesis, transfer, and degradation process of the MoS_2 crystals. **b**–**d** OM images and Raman and PL spectra of the MoS_2 crystals synthesized on SiO_2/Si and transferred to SU-8/sapphire substrates. **e**–**g** OM, AFM, and SHG mapping images of the monolayer MoS_2 crystals with different misorientation angles (from 0° to 55°) on SU-8/sapphire substrates before degradation. The arrows in **e** indicate the orientations of each crystal

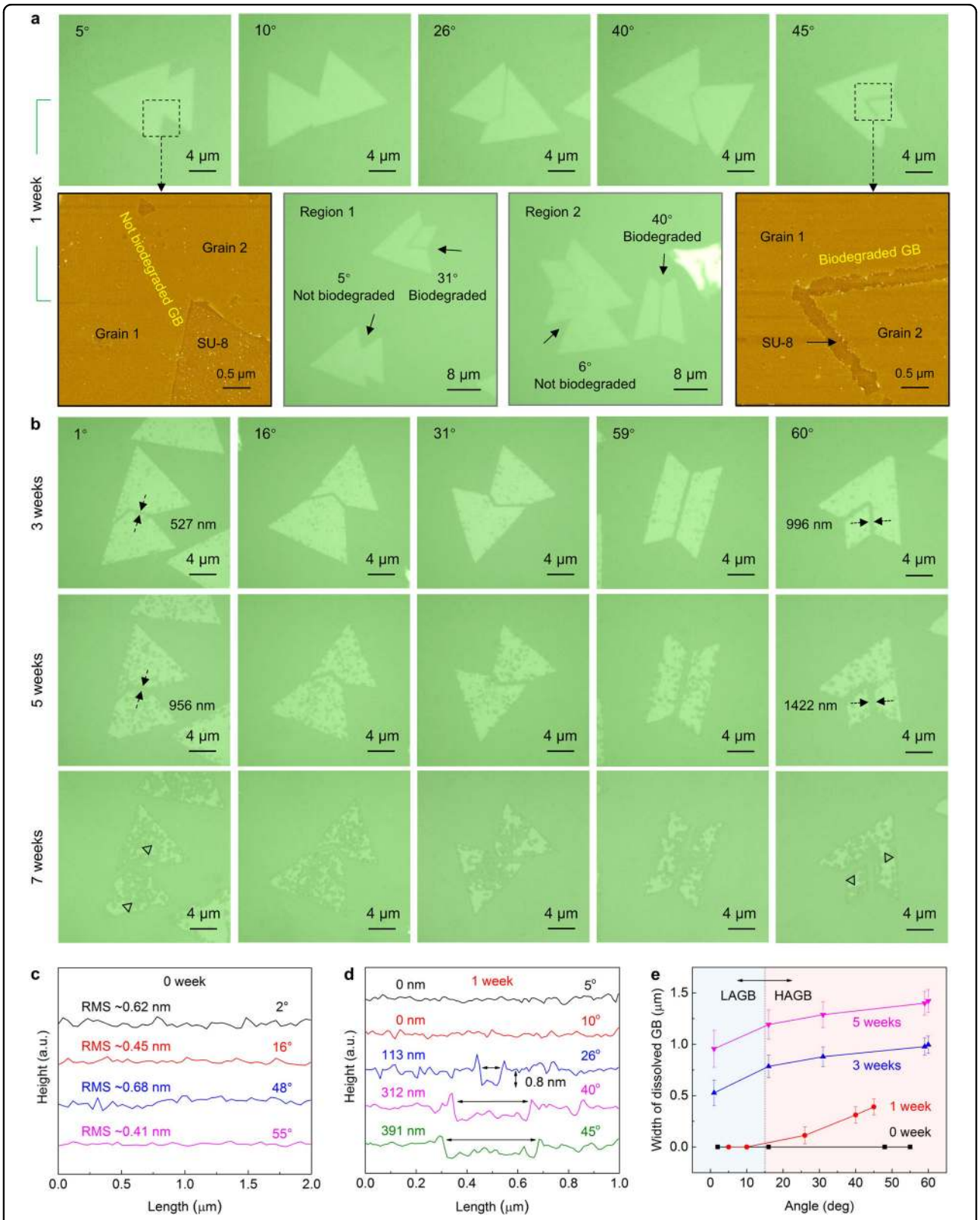

Fig. 2 Angle-dependent selective degradation of CVD-grown monolayer MoS_2 crystals in PBS solution. a OM and AFM images of the MoS_2 crystals with different misorientation angles (from 5° to 45°) after the crystals were kept in PBS solution (pH 7.4, 75 °C) for 1 week. **b** OM images of the MoS_2 crystals with different misorientation angles (from 1° to 60°) after the crystals were kept in PBS solution (pH 7.4, 75 °C) for 2–7 weeks. **c**, **d** AFM height profiles across the MoS_2 GB regions before and after degradation for 1 week. **e** The width of dissolved MoS_2 GB regions determined by both misorientation angles (from 1° to 60°) and degradation time (0–5 weeks)

and the adjacent grains were separated accordingly. However, surprisingly, the MoS_2 GBs with angles of 5° or 10° were well preserved, and two contiguous grains were still connected (Fig. 2a). Such different degradation results between LAGBs and HAGBs were further confirmed in the magnified AFM images of the 5° and 45° samples, where differences were easily observed in arbitrary regions (bottom of Fig. 2a). These observations indicate that the degradation process preferentially initiates at the HAGBs rather than at the LAGBs. This unique phenomenon, which we refer to as "angle-dependent selective degradation", has never been observed or previously reported in oxidation studies of MoS_2[13,14,24]. To demonstrate this concept, a high-temperature oxidation test of monolayer MoS_2 crystals was performed on an SiO_2 substrate by heating the crystals on a hot plate at 380 °C in air for various time intervals (from 90 to 210 min) (Supplementary Figure S2). After 90 min, the MoS_2 GBs with angles of 6°, 23°, or 56° were etched with similar widths, indicating that the angle-dependent selective degradation of MoS_2 GBs did not occur at an elevated temperature. By contrast, the aqueous system can provide ions with water and oxygen molecules and transport them away as products, which is impossible in the dry state. In addition, high-temperature oxidation may be limited by diffusion, rather than the elementary reactions themselves. The possible reactions that could have occurred during the degradation process are as follows:

$$2MoS_2 + 7O_2 \rightarrow 2MoO_3 + 4SO_2, \quad (1)$$

$$MoO_3 + 2OH^- \rightarrow MoO_4^{2-} + H_2O, \quad (2)$$

$$MoS_2 + 9/2O_2 + 3H_2O \rightarrow MoO_4^{2-} + 2SO_4^{2-} + 6H^+, \quad (3)$$

where the molybdate ion (MoO_4^{2-}) is the main Mo-containing byproduct, which has been confirmed by inductively coupled plasma-mass spectrometry (ICP-MS) measurements[20,26,27]. Note that Na^+ and K^+ ions in the PBS solution may lead to lattice distortions of MoS_2 and the formation of Na_2S (from 2H-MoS_2 to 1T-$NaMoS_2$ and then to soluble Na_2S), further accelerating the degradation process[20]. According to the OM images presented in Fig. 2b, both the LAGBs and the HAGBs degraded after 3 weeks; the degradation of the whole MoS_2 grain also began, as evidenced by the numerous small pits observed inside the grains. Five weeks later, the degraded GB regions became wider, and the pits were enlarged. After 7 weeks, the MoS_2 GB regions were not easily observed. The pits merged into each other to form larger ones, and some of them even exhibited triangular-shaped pits whose orientation was opposite to that of the parent grains. These trends indicate that the MoS_2 crystals would be completely degraded in the PBS solution in a sufficient amount of time (e.g., more than 10 weeks). This process represents the entire degradation process of CVD-grown monolayer 2H-MoS_2 crystals in PBS solution.

To elucidate the degradation speed of monolayer MoS_2 crystals, the width of the degraded GB regions was measured using AFM. Figure 2c represents the height profiles across the MoS_2 GBs with angles of 2°, 16°, 48°, or 55° before degradation (Fig. 1f, Supplementary Figure S3). At this stage, two grains were connected without any space between them. The RMS roughness of each GB was found to be in the normal range (0.41–0.68 nm). The MoS_2 GBs with angles of 5° or 10° were still intact after 1 week; however, the MoS_2 GBs with angles of 26°, 40°, or 45° were selectively degraded, with gap widths of 113, 312, or 391 nm, respectively (Fig. 2d). These results indicate that the higher the HAGB angle, the higher the degradation speed. They also imply that a continuous MoS_2 monolayer with a small grain size exhibits the highest degradation rate because most of them contain HAGBs[20,44]. After 3 weeks, the width of degraded GBs increased from 527 (1°) to 996 nm (60°); 5 weeks later, they had further enlarged to between 956 (1°) and 1422 nm (60°) (Fig. 2e). The angle-dependent selective degradation occurred in the early stage (in 3 weeks or less). After both the LAGBs and HAGBs were degraded, the degradation speed of the GB regions in the lateral direction was approximately the same (~213 nm per week), as shown in Fig. 2e. Because such selective degradation started at the very beginning, HAGBs could maintain a higher speed than LAGBs, which enables control of the lifetime in biofluids via the selection of MoS_2 crystals with different misorientation angles.

Interestingly, the edges of the MoS_2 crystals were not degraded from the outside in, and the size of each crystal did not obviously decrease after 3–5 weeks (Fig. 2b). The Mo-rich synthesis condition applied in this study contributes to the formation of monolayer MoS_2 crystals with sharp, straight, and Mo zigzag edges[30]. Calculations show that the surface energy σ of a Mo zigzag edge remains smaller than that of an S zigzag edge provided that the chemical potential of sulfur (μ_S) is <-1.65 eV. The lower surface energy of a Mo zigzag edge makes it much more stable than an S edge; thus, Mo zigzag edges will be more abundant than S zigzag edges under any realistic conditions[48]. This greater abundance of Mo zigzag edges leads to their slow degradation in PBS solution compared with the degradation rates of grains or GBs. Because the center of the crystal may contain a high defect density, particularly in the form of S vacancies, degradation of the crystal occurs predominantly at these sites. This degradation

process further accelerates with increasing time, and finally the crystal disappears, leaving behind some part of the crystal (Mo zigzag) edge intact at the substrate even after 5 weeks (Fig. 2b). Notably, the phenomenon of angle-dependent selective degradation is statistically significant in our research and could also be observed when the temperature of the PBS solution was reduced from 75 °C to 40 °C (very close to physiological conditions, 37 °C). The main difference is that the degradation process becomes much slower (approximately one-tenth of that at 75 °C) (Supplementary Figure S4). In addition, due to the same synthesis conditions, isolated monolayer MoS_2 crystals with a triangular shape degrade with the same tendency and speed as the polycrystalline domains (Supplementary Figure S5).

To discover the structural cause of the angle-dependent selective degradation and reveal the relation between atomic structures and degradation behaviors, TEM and STEM characterizations are performed for CVD-grown monolayer MoS_2 crystals with different misorientation angles. The high-angle annular dark-field STEM (HAADF-STEM) images of the MoS_2 crystals with angles of 5°, 16°, 27°, and 60° suspended on quantifoil TEM grids are presented in Fig. 3a. The equilateral geometry of the triangular crystals, together with sharp and straight edges, implies that the MoS_2 crystals are single crystalline (the semiconducting 2H phase) and may well have Mo-terminated edges[11,30]. Fig. 3b shows the dark-field TEM (DF-TEM) images and selected-area electron-diffraction (SAED) patterns taken from the regions marked with circles in Fig. 3a. GBs are formed between two adjacent grains (Grains 1 and 2), and their distributions are consistent with the SHG results in Fig. 1g. The corresponding SAED patterns inset in Fig. 3b have two sets of hexagonally arranged diffraction spots, which rotate gradually from one to the other because of the increment in the misorientation angle[31]. To examine the atomic structure along the GBs, atomically resolved HAADF-STEM was performed. Figure 3c presents the HAADF-STEM images corresponding to the areas (marked with a circle) of the four GBs in Fig. 3b.

Based on these high-resolution images, three pieces of information can be obtained. First, the MoS_2 crystals with a hexagonal lattice and no Moiré pattern have a monolayer structure. The brighter spots are the Mo atoms, and the darker spots are the two stacked S atoms because the contrast of HAADF-STEM images scales approximately as the square of the atomic number[31]. Second, the higher the misorientation angle, the greater the number of localized defects generated along the GBs, including Mo dangling bonds and tiny holes. These dangling bonds and holes are mainly caused by the incomplete growth of GBs or by slight aging because of the storage process[13,33]. Third, a similar number of point defects (V_S and V_{S2}) whose edges are along zigzag directions (Mo-oriented) are observed in each crystal. They are inevitable in MoS_2 crystals, as suggested by the second law of thermodynamics, and are more noticeable in CVD-grown samples because of imperfections introduced during the growth process[37]. Vacancies V_S and V_{S2} have been reported to have the lowest formation energies (ΔE_{Form}) of 2.12 and 4.14 eV, respectively, among all of the defects; here, $\Delta E_{Form} = \Delta E_{System} - N_S \times N_{S\_ML} - N_{Mo} \times N_{Mo\_ML}$, where N_{S_ML} and N_{Mo_ML} are the single-atom energy of Mo and S, respectively, in a perfect monolayer. The results show that S-deficient CVD-grown monolayer MoS_2 preferentially forms S vacancies, indicating that V_S is the most common defect, followed by V_{S2}[39]. The existence of such vacancies can substantially reduce the dissociation kinetic barrier by half, from ~1.56 to ~0.8 eV[14], and make the defect regions in biofluids easier to degrade.

According to the magnified HAADF-STEM images from the continuous GB regions in Fig. 3c, more information about the evolution of edge structures and dislocations can be collected (Fig. 3d). In the LAGB case (5°), two adjacent grains with armchair edges meet and combine well with no dislocation because their complementary structures lead to the generation of new hexagonal lattices at the center and connect as one crystal in local areas. In the HAGB cases (16° and 27°), however, two grains, one an armchair edge and the other with a zigzag edge, cannot perfectly and stably combine. Thus, Mo-oriented dislocations, such as 5|7-fold ring cores, are formed to facilitate the transition from one edge to the other[30,32]. When the angle increases from 16° to 27°, the lattice mismatch becomes larger, and more 5|7-fold ring cores are generated (from 2 to 3). When the angle approaches 60°, two grains with zigzag edges come face to face, and the 5|7-fold ring cores change into 4|4-fold ring cores, although the number of cores does not change noticeably. Based on the above results, the angle-dependent evolvement rules about edge structures and dislocations along the MoS_2 GBs can be determined, as shown in Fig. 3e, f.

In general, from LAGBs to HAGBs, such increase in dislocation number and changes in dislocation type mainly result from the various levels of lattice mismatch between two neighboring grains, which are fundamentally decided by the related edge structures (armchair or zigzag). For a perfect monolayer MoS_2, Mo atoms are sandwiched and protected by top and bottom S atoms with no broken lattice, preventing the interaction or reaction between 2D MoS_2 and the biofluid to a certain extent. This lack of interaction causes some parts of the MoS_2 crystals to remain intact even after 7 weeks in PBS solution (Fig. 2b). Because of these GBs and point defects, CVD-grown monolayer MoS_2 crystals have different

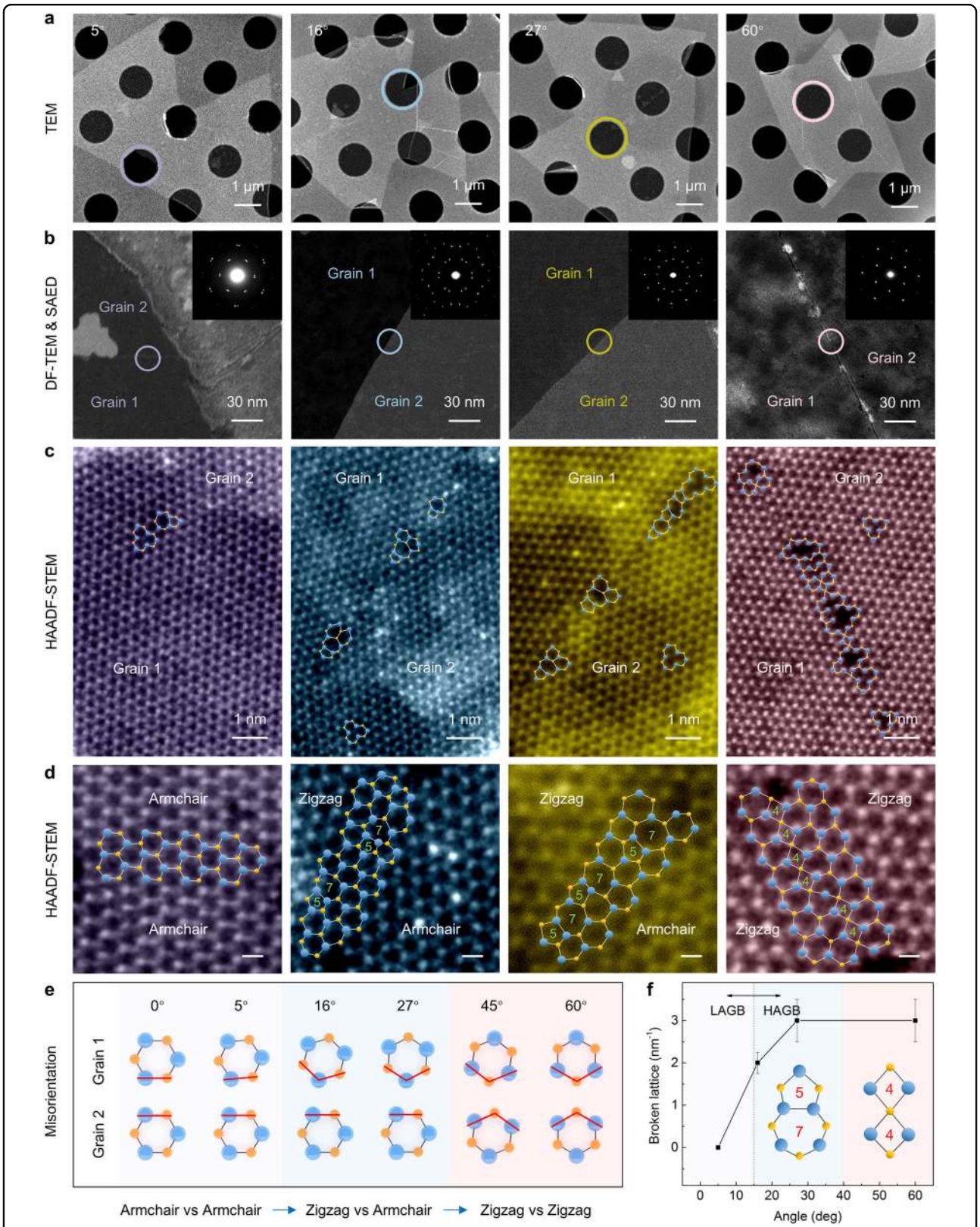

Fig. 3 TEM characterization of monolayer MoS_2 crystals with different misorientation angles. a TEM images of the MoS_2 crystals with four different angles (from 5° to 60°) suspended on Quantifoil TEM grids. **b** DF-TEM images of the MoS_2 crystals taken at the locations marked in **a**. Insets are the corresponding SAED patterns. **c**, **d** HAADF-STEM images of the related MoS_2 GBs, as obtained from the locations marked in **b**. Scale bar in **d**: 0.25 nm. **e** Schematics of the edge structure evolution between two adjacent grains when the misorientation angle increases from 5° to 60°. **f** The number of broken lattices per unit distance (1 nm) along the GBs gained from **d**

quantities of dangling bonds, which result from the growth conditions and misorientation angle. The related GB energy is proportional to the tilt angle because large tilt angles result in higher dislocation densities[32]. Such dangling bonds reduce the stability and enhance the chemical activity of these areas: more dangling bonds result in greater reactivity[38,41,42,49]. Therefore, HAGBs with more dangling bonds, holes, and ring cores exhibit faster degradation in PBS solution compared with LAGBs with fewer dangling bonds, holes, and ring cores, leading to the phenomenon of angle-dependent selective degradation. In the same manner, point defects exhibit much slower degradation than GBs because they lack sufficient dangling bonds. Above all, the degradation process of monolayer MoS_2 crystals in PBS solution is induced by intrinsic defects in the grains or along the GBs. This degradation process is suppressed in the unbroken regions, whereas it readily occurs in the regions with high defect densities.

As a starting point of the degradation process, the intrinsic defects in monolayer MoS_2 crystals play important roles in determining the time and range of degradation. However, the sequence of steps in this process needs to be discussed to determine the corresponding behaviors of these defects. Figure 4a presents the OM and AFM images of degraded MoS_2 crystals with an LAGB (1°) and a HAGB (60°) after the crystals were exposed to PBS solution for 3 weeks. Notably, the shapes of the degraded LAGB and HAGB crystals differ. The former consists of a wedge shape, whereas the latter

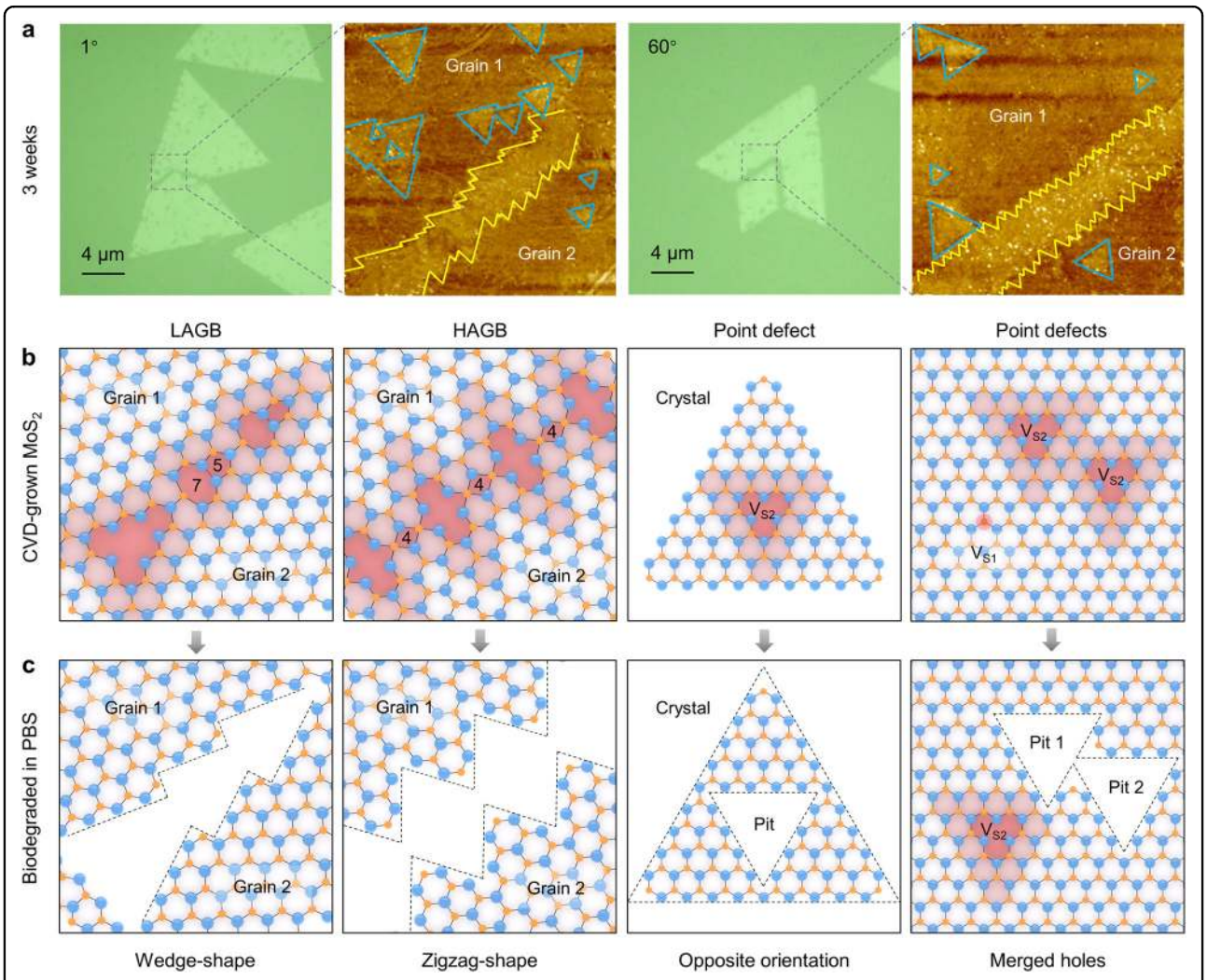

Fig. 4 Degradation behaviors and mechanisms of CVD-grown monolayer MoS_2 crystals in PBS solution. a OM and AFM images of the monolayer MoS_2 crystals with low-angle (1°) and high-angle (60°) GBs after accelerated degradation in PBS solution at 75 °C for 3 weeks. **b**, **c** Schematics of the degradation behaviors and mechanisms of monolayer MoS_2 crystals with four types of dislocations and defects, including LAGBs, HAGBs, single-point defects, and multiple-point defects

consists of a zigzag shape. In addition, many triangular pits are generated inside the crystals; some are isolated, whereas others are connected. More interestingly, the orientation of each pit is consistent with the others but opposite to the orientation of the parent crystals. Before exploring these unusual results, we first note that LAGB and HAGB have 5|7-fold and 4|4-fold ring cores, together with their variations, Mo dangling bonds, and tiny holes. Meanwhile, V_S and V_{S2} are the main point defects in the crystals. Based on these structures, we established four sets of models to explain the formation of the edges and pits.

Figure 4b, c demonstrate the models corresponding to LAGBs, HAGBs, single-point defects, and multiple-point defects before and after degradation. The LAGB is composed of 5|7-fold ring cores and variations in a wedge shape, and the HAGB is composed of 4|4-fold ring cores and variations in a zigzag shape (Fig. 4b). After the crystals were placed in PBS solution for a certain time, these fundamental shapes extended out of the lattice perpendicular to the zigzag edges and became larger, although their general shapes remained unchanged (wedge or zigzag) (Fig. 4c). When the reaction time was sufficiently long, the GB regions with two different shapes extended from the nanoscale into the microscale and were observed with the aid of OM, which is consistent with the experimental results shown in Fig. 4a. Thus, the final shape of the degraded GBs is decided by the original shape of the dislocations along the GBs. The degradation process favors dislocations perpendicular to the zigzag Mo edge because of their higher activity compared with dislocations perpendicular to the zigzag S edge or armchair edge[24,42]. Similarly, V_{S2} has an initial triangular shape, opposite to that of the parent crystal, leading to the formation of a large triangular hole with the same orientation as V_{S2}. In the event of two adjacent V_{S2}, the corresponding final pits will be connected or even combined, which accelerates the degradation of MoS_2 grains. Because V_S has fewer dangling bonds than V_{S2}, it does not degrade easily, and the process is delayed in this area, resulting in a smaller triangular hole than the one that resulted from V_{S2} (Fig. 4c). Due to this variation in hole size, the sizes of pits in degraded MoS_2 grains vary from small to large (Fig. 4a).

Generally, the MoS_2 surface is kinetically stable with respect to oxidation at low temperatures, and the barrier at broken edges is much lower; hence, oxidation and degradation readily occur at such sites. In addition, the formation of MoO_3 groups leads to the addition of oxygen atoms at the broken edge, continuing the oxidation and degradation process[48]. In some respects, imperfections, such as dislocations and point defects, in CVD-grown monolayer MoS_2 crystals strongly influence the degradation process, which could potentially be further controlled by defect or domain size engineering in the future[42,50]. For instance, vacancies can be created or healed to modulate the defect density and degradation speed of monolayer MoS_2 via synthetic or post-processing technologies. The degradation of monolayer MoS_2 crystals is affected not only by external conditions, such as solution concentration, pH, and temperature, but also by internal factors, such as grain size, GB angle, and defect density, which can be modulated via the synthesis conditions.

Conclusions

To summarize, the degradation of CVD-grown monolayer MoS_2 crystals with different misorientation angles in PBS solution is elucidated, and the morphological transformation, degradation behaviors, and structural cause are systematically investigated using OM, AFM, TEM, and STEM. The degradation process of MoS_2 crystals is evidenced to be induced by intrinsic defects in the as-grown crystals, including GBs and point defects, because of the greater density of dangling bonds and higher reactivity in these regions. We also introduced the phenomenon of angle-dependent selective degradation, which explains that HAGBs are degraded preferentially at a faster rate than LAGBs because HAGBs contain more 5|7- and 4|4-fold ring cores, together with more tiny holes, due to the greater lattice mismatch between two adjacent grains. Once begun, the degradation process extends perpendicular to the zigzag edge of LAGBs, HAGBs, V_S, and V_{S2}, resulting in broken edges in a wedge or zigzag shape and triangular pits with opposite orientation to the parent crystals. These triangular pits merge into each other, resulting in the complete degradation of monolayer MoS_2 crystals. Such a defect-induced degradation process can be further controlled via defect engineering methods, such as intrinsic or artificial defect modulation. MoS_2 is only one member of a large family of 2D TMDCs; the achievements here provide a template for exploring the degradation of other 2D TMDCs in biofluids and suggest their promising applications in bioabsorbable devices and systems with controlled lifetime and performance, obviating the requirement for surgical retrieval and eliminating solid electronic waste.

Acknowledgements

This work was supported by the National Research Foundation of Korea (NRF) funded by the Korean government (MSIT) (NRF-2015R1A3A2066337).

Author details

[1]School of Electrical and Electronic Engineering, Yonsei University, 50 Yonsei-ro, Seodaemun-gu, Seoul 03722, Republic of Korea. [2]School of Materials Science and Engineering, Ulsan National Institute of Science and Technology (UNIST), 50 UNIST-gil, Ulju-gun, Ulsan 44919, Republic of Korea. [3]Division of Nano & Energy Convergence Research, Daegu Gyeongbuk Institute of Science and Technology (DGIST), 333 Techno jungang-daero, Hyeonpung-myeon, Dalseong-gun, Daegu 711873, Republic of Korea

Conflict of interest
The authors declare that they have no conflict of interest.

Publisher's note
Springer Nature remains neutral with regard to jurisdictional claims in published maps and institutional affiliations.

Supplementary information is available for this paper at https://doi.org/10.1038/s41427-018-0078-6.

Received: 26 May 2018 Revised: 8 July 2018 Accepted: 10 July 2018.
Published online: 22 August 2018

References

1. Solis-Fernandez, P., Bissett, M. & Ago, H. Synthesis, structure and applications of graphene-based 2D heterostructures. *Chem. Soc. Rev.* **46**, 4572 (2017).
2. Tan, C. et al. Recent advances in ultrathin two-dimensional nanomaterials. *Chem. Rev.* **117**, 6225 (2017).
3. Appel, J. H. et al. Low cytotoxicity and genotoxicity of two-dimensional MoS_2 and WS_2. *ACS Biomater. Sci. Eng.* **2**, 361 (2016).
4. Lu, Q., Yu, Y., Ma, Q., Chen, B. & Zhang, H. 2D transition-metal-dichalcogenide-nanosheet-based composites for photocatalytic and electrocatalytic hydrogen evolution reactions. *Adv. Mater.* **28**, 1917 (2016).
5. Wang, Z. et al. Biological and environmental interactions of emerging two-dimensional nanomaterials. *Chem. Soc. Rev.* **45**, 1750 (2016).
6. Wu, Y. C. et al. Extrinsic origin of persistent photoconductivity in monolayer MoS_2 field effect transistors. *Sci. Rep.* **5**, 11472 (2015).
7. Choi, G. J. et al. Polarized light-emitting diodes based on patterned MoS_2 nanosheet hole transport layer. *Adv. Mater.* **29**, 1702598 (2017).
8. Lee, Y. H. et al. Synthesis of large-area MoS_2 atomic layers with chemical vapor deposition. *Adv. Mater.* **24**, 2320 (2012).
9. Chen, X. et al. Lithography-free plasma-induced patterned growth of MoS_2 and its heterojunction with graphene. *Nanoscale* **8**, 15181 (2016).
10. Miseikis, V. et al. Rapid CVD growth of millimetre-sized single crystal graphene using a cold-wall reactor. *2D Mater.* **2**, 014006 (2015).
11. Yang, H. et al. Highly scalable synthesis of MoS_2 thin films with precise thickness control via polymer-assisted deposition. *Chem. Mater.* **29**, 5772 (2017).
12. Zhou, H. et al. Thickness-dependent patterning of MoS_2 sheets with well-oriented triangular pits by heating in air. *Nano Res.* **6**, 703 (2013).
13. Gao, J. et al. Aging of transition metal dichalcogenide monolayers. *ACS Nano* **10**, 2628 (2016).
14. Kc, S., Longo, R. C., Wallace, R. M. & Cho, K. Surface oxidation energetics and kinetics on MoS_2 monolayer. *J. Appl. Phys.* **117**, 135301 (2015).
15. Zhang, X., Jia, F., Yang, B. & Song, S. Oxidation of molybdenum disulfide sheet in water under in situ atomic force microscopy observation. *J. Phys. Chem. C* **121**, 9938 (2017).
16. Fu, K. K., Wang, Z., Dai, J., Carter, M. & Hu, L. Transient electronics: materials and devices. *Chem. Mater.* **28**, 3527 (2016).
17. Cheng, H. & Vepachedu, V. Recent development of transient electronics. *Appl. Mech. Lett.* **6**, 21 (2016).
18. Kang, S. K. et al. Bioresorbable silicon electronic sensors for the brain. *Nature* **530**, 71 (2016).
19. Yu, K. J. et al. Bioresorbable silicon electronics for transient spatiotemporal mapping of electrical activity from the cerebral cortex. *Nat. Mater.* **15**, 782 (2016).
20. Chen, X. et al. CVD-grown monolayer MoS_2 in bioabsorbable electronics and biosensors. *Nat. Commun.* **9**, 1690 (2018).
21. Yamamoto, M., Einstein, T. L., Fuhrer, M. S. & Cullen, W. G. Anisotropic etching of atomically thin MoS_2. *J. Phys. Chem. C* **117**, 25643 (2013).
22. Ionescu, R. et al. Oxygen etching of thick MoS_2 films. *Chem. Commun.* **50**, 11226 (2014).
23. Parzinger, E. et al. Photocatalytic stability of single- and few-layer MoS_2. *ACS Nano* **9**, 11302 (2015).
24. Lv, D. et al. Atomic process of oxidative etching in monolayer molybdenum disulfide. *Sci. Bull.* **62**, 846 (2017).
25. Longo, R. C. et al. Intrinsic air stability mechanisms of two-dimensional transition metal dichalcogenide surfaces: basal versus edge oxidation. *2D Mater.* **4**, 025050 (2017).
26. Wang, Z. et al. Chemical dissolution pathways of MoS_2 nanosheets in biological and environmental media. *Environ. Sci. Technol.* **50**, 7208 (2016).
27. Kurapati, R. et al. Enzymatic biodegradability of pristine and functionalized transition metal dichalcogenide MoS_2 nanosheets. *Adv. Funct. Mater.* **27**, 1605176 (2017).
28. Kalantar-zadeh, K. et al. Two-dimensional transition metal dichalcogenides in biosystems. *Adv. Funct. Mater.* **25**, 5086 (2015).
29. Gan, X., Zhao, H. & Quan, X. Two-dimensional MoS_2: a promising building block for biosensors. *Biosens. Bioelectron.* **89**, 56 (2017).
30. van der Zande, A. M. et al. Grains and grain boundaries in highly crystalline monolayer molybdenum disulphide. *Nat. Mater.* **12**, 554 (2013).
31. Najmaei, S. et al. Vapour phase growth and grain boundary structure of molybdenum disulphide atomic layers. *Nat. Mater.* **12**, 754 (2013).
32. Zou, X., Liu, Y. & Yakobson, B. I. Predicting dislocations and grain boundaries in two-dimensional metal-disulfides from the first principles. *Nano Lett.* **13**, 253 (2013).
33. Cheng, J. et al. Kinetic nature of grain boundary formation in as-grown MoS_2 monolayers. *Adv. Mater.* **27**, 4069 (2015).
34. Artyukhov, V. I., Hu, Z., Zhang, Z. & Yakobson, B. I. Topochemistry of bowtie- and star-shaped metal dichalcogenide nanoisland formation. *Nano Lett.* **16**, 3696 (2016).
35. Ly, T. H. et al. Misorientation-angle-dependent electrical transport across molybdenum disulfide grain boundaries. *Nat. Commun.* **7**, 10426 (2016).
36. Park, S. et al. Spectroscopic visualization of grain boundaries of monolayer molybdenum disulfide by stacking bilayers. *ACS Nano* **9**, 11042 (2015).
37. Zhou, W. et al. Intrinsic structural defects in monolayer molybdenum disulfide. *Nano Lett.* **13**, 2615 (2013).
38. Rasool, H. I., Ophus, C. & Zettl, A. Atomic defects in two dimensional materials. *Adv. Mater.* **27**, 5771 (2015).
39. Hong, J. et al. Exploring atomic defects in molybdenum disulphide monolayers. *Nat. Commun.* **6**, 6293 (2015).
40. Islam, M. R. et al. Tuning the electrical property via defect engineering of single layer MoS_2 by oxygen plasma. *Nanoscale* **6**, 10033 (2014).
41. Li, H. et al. Activating and optimizing MoS_2 basal planes for hydrogen evolution through the formation of strained sulphur vacancies. *Nat. Mater.* **15**, 48 (2016).
42. Lin, Z. et al. Defect engineering of two-dimensional transition metal dichalcogenides. *2D Mater.* **3**, 022002 (2016).
43. Hong, J., Jin, C., Yuan, J. & Zhang, Z. Atomic defects in two-dimensional materials: from single-atom spectroscopy to functionalities in opto-/electronics, nanomagnetism, and catalysis. *Adv. Mater.* **29**, 1606434 (2017).
44. Ly, T. H. et al. Observing grain boundaries in CVD-grown monolayer transition metal dichalcogenides. *ACS Nano* **8**, 11401 (2014).
45. Shehzad, M. A. et al. Study of grains and boundaries of molybdenum diselenide and tungsten diselenide using liquid crystal. *Nano Lett.* **17**, 1474 (2017).
46. Li, Y. et al. Probing symmetry properties of few-layer MoS_2 and h-BN by optical second-harmonic generation. *Nano Lett.* **13**, 3329 (2013).
47. Yin, L. et al. Mechanisms for hydrolysis of silicon nanomembranes as used in bioresorbable electronics. *Adv. Mater.* **27**, 1857 (2015).
48. Martincova, J., Otyepka, M. & Lazar, P. Is single layer MoS_2 stable in the air? *Chemistry* **23**, 13233 (2017).
49. González, C., Dappe, Y. J. & Biel, B. Reactivity enhancement and fingerprints of point defects on a MoS_2 monolayer assessed by ab initio atomic force microscopy. *J. Phys. Chem. C* **120**, 17115 (2016).
50. Liscio, A. et al. Evolution of the size and shape of 2D nanosheets during ultrasonic fragmentation. *2D Mater.* **4**, 025017 (2017).